Inorganic Chemistry

Article

Cite This: Inorg. Chem. 2017, 56, 7120-7126

pubs.acs.org/IC

Covalent Co–O–V and Sb–N Bonds Enable Polyoxovanadate Charge Control

Maren Rasmussen,[†] Christian Näther,[†] Jan van Leusen,[‡] Paul Kögerler,[‡] Lyuben Zhechkov,[§] Thoma Heine,[§] and Wolfgang Bensch*[,†]

[†]Institut für Anorganische Chemie, Christian-Albrechts-Universität Kiel, D-24118 Kiel, Germany

[‡]Institut für Anorganische Chemie, RWTH Aachen, D-52074 Aachen, Germany

[§]Wilhelm-Ostwald-Institut für Physikalische und Theoretische Chemie, Universität Leipzig, D-04103 Leipzig, Germany

Supporting Information

ABSTRACT: The formation of $[\{Co^{II}(teta)_2\}\{Co^{II}_2(tren)(teta)_2\}V^{IV}_{15}Sb^{III}_6O_{42}(H_2O)]\cdot ca.9H_2O$ [teta = triethylenetetraamine; tren = tris(2-aminoethyl)amine] illustrates a strategy toward reducing the molecular charge of polyoxovanadates, a key challenge in their use as components in single-molecule electronics. Here, a V–O–Co bond to a binuclear Co^{2+}-centered complex and a Sb–N bond to the terminal N atom of a teta ligand of a mononuclear Co^{2+} complex allow for full charge compensation of the archetypal molecular magnet $[V_{15}Sb_6O_{42}(H_2O)]^{6-}$. Density functional theory based electron localization function analysis demonstrates that the Sb–N bond has an electron density similar to that of a Sb–O bond. Magnetic exchange coupling between the V^{IV} and Co^{II} spin centers mediated via the Sb–N bridge is comparably weakly antiferromagnetic.

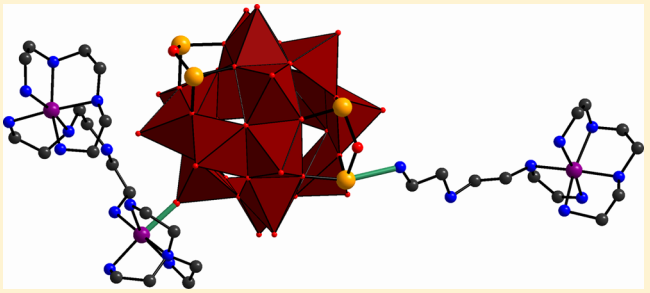

INTRODUCTION

Polyoxovanadates incorporating antimony (Sb-POVs) and other semimetal constituents represent a comparably new and rapidly growing class of molecular metal oxide compounds, enabling various subsequent functionalization methods relevant to materials chemistry.[1] In light of their versatile redox chemistry, polyoxovanadates (POVs) are currently extensively studied for their use in single-molecule electronics and spintronics. In this context, single-molecule charge-transport experiments, e.g., in scanning tunneling microscopy (STM), are of particular interest but are frequently hampered by the high charge of the polyanions. The surface deposition of highly charged polyanions and their countercations often results in aggregation and random association of the cluster anions with countercations, which greatly complicates STM analysis. We thus are exploring routes to charge-neutral derivatives and herein present a prototypal system in which cationic groups are covalently linked to both the Sb and V centers of an Sb-POV.

First reports of POVs chemically modified by Sb, specifically $[V_{14}{}^{IV}Sb_8{}^{III}O_{42}(H_2O)]^{4-}$ anions, date back to 2002 and 2004.[2,3] A less Sb-rich cluster anion with composition $[V_{16}Sb_4O_{42}]^{4-}$ was first observed in $(C_6H_{17}N_3)_4[V_{16}Sb_4O_{42}]\cdot 2H_2O$ ($C_6H_{17}N_3$ = double-protonated 2-piperazine-*N*-ethylamine), which was also prepared under solvothermal conditions.[4] The structural family of Sb-POVs with the general formula $[(amineH)_mV_{18-z}Sb_{2z}O_{42}]\cdot nH_2O$ (z = 2–4) was completed by a new member with composition $(trenH_3)_2[V_{15}Sb_6O_{42}]\cdot 0.33tren\cdot nH_2O$ [n = 3–5; tren = tris(2-aminoethyl)amine][5] containing the first antimony analogue of the $[V_{15}As_6O_{42}(H_2O)]^{6-}$ molecular magnet.[6] The structure of the $[V^{IV}_{15}Sb_6O_{42}]^{6-}$ polyoxoanion can be regarded as a derivative of the $\{V_{18}O_{42}\}$ archetype when three $\{VO_5\}$ square pyramids are replaced by three dumbbell-like $\{Sb_2O_5\}$ units. In the solid-state structure of $(trenH_3)_2[V_{15}Sb_6O_{42}]\cdot 0.33tren\cdot nH_2O$, weak intercluster interactions lead to the formation of a trimeric superstructure $([V^{IV}_{15}Sb_6O_{42}]^{6-})_3$. The Sb-POVs were chemically modified by covalent decoration, with transition-metal complexes like in $[V_{16}Sb_4O_{42}(H_2O)\{VO(C_6H_{14}N_2)_2\}_4]\cdot 10H_2O\cdot C_6H_{14}N_2$ [$C_6H_{14}N_2$ = (±)-*trans*-1,2-diaminocyclohexane] displaying a neutral Sb-POV building block with two opposite $\{Sb_2O_5\}$ groups replacing two $\{VO_5\}$ square pyramids. The anion is further expanded by four square-pyramidal $[V^{IV}O(C_6H_{14}N_2)_2]^{2+}$ complexes, thus leading to a charge-neutral compound.[7] There are two examples for the functionalization of Sb-POVs with organic molecules,[8] with the anions $[V^{IV}_{14}Sb_8O_{42}(H_2O)]^{4-}$ and $[V^{IV}_{15}Sb_6O_{42}(H_2O)]^{6-}$ displaying covalent bonds to the ammonium cations $(C_6H_{15}N_3)^+$ with Sb–N bonds from 2.502 to 2.542 Å. Further chemical modification by Zn^{2+}-centered complexes was also achieved,[9] leading to 1D chains formed by alternating complexes and polyoxoanions. A $[V^{IV}_{16}Sb_4O_{42}(H_2O)]^{8-}$ anion with reduced symmetry of the $\{V_{16}\}$ skeleton from D_{2h} to C_2 was reported recently.[10] The structural chemistry of Sb-POVs was enhanced

Received: March 27, 2017
Published: May 25, 2017

DOI: 10.1021/acs.inorgchem.7b00724
Inorg. Chem. 2017, 56, 7120–7126

by the covalent attachment of Co^{2+}-centered complexes like $[Co(tren)(H_2O)]^{2+}$, $[Co_2(tren)_3]^{4+}$, $[Co(tren)(en)]^{2+}$, $[Co(tren)_2]^{2+}$, and $[Co(tren)(trenH_2)]^{4+}$ moieties to the Sb-POV anions.[11] Relatively short intercluster Sb···O distances were found in $(enH_2)_2[V^{IV}_{14}Sb_8O_{42}(H_2O)]\cdot 3H_2O$ and $(ppzH_2)_2[V^{IV}_{14}Sb_8O_{42}(H_2O)]$ (ppz = piperazine).[12] Remarkable structural differences were observed between $[Co(C_5H_{15}N_3)_2]_2[\{Co(C_5H_{15}N_3)_2\}V_{15}Sb_6O_{42}(H_2O)]\cdot 5H_2O$ and $[Ni(C_5H_{15}N_3)_2]_2[\{Ni(C_5H_{15}N_3)_2\}V_{15}Sb_6O_{42}(H_2O)]\cdot 8H_2O$ [$C_5H_{15}N_3$ = *N*-(2-aminoethyl)-1,3-propanediamine]:[13] in the former structure, the anions are connected through weak intercluster Sb···O interactions, while Sb···N contacts are observed for the latter. Dimeric $\{[Ni_2(tren)_3(V_{15}Sb_6O_{42}(H_2O)_{0.5})]_2\}^{4-}$ fragments were found in $[Ni(trenH)_2][Ni_2(tren)_3(V_{15}Sb_6O_{42}(H_2O)_{0.5})]_2\cdot H_2O$ containing in situ produced $[Ni_2(tren)_3]^{4+}$ complexes.[14] Adjusting the reaction temperature afforded the crystallization of two pseudopolymorphic compounds with compositions $[Ni(dien)_2]_3[V_{15}Sb_6O_{42}(H_2O)]\cdot nH_2O$ (n = 12 and 8).[15] The two pseudopolymorphs differ in the occurrence of $\{Ni(dien)_2\}^{2+}$ complexes adopting the *s-fac*, *mer*, and *u-fac* configurations in one compound and only a *mer*-$\{Ni(dien)_2\}^{2+}$ complex in the other compound. Finally, a unique 3D network was observed in the structure of $[\{Fe(C_6H_{14}N_2)_2\}_3\{V_{15}Sb_6O_{42}(H_2O)\}]\cdot 8H_2O$ ($C_6H_{14}N_2$ = *trans*-1,2-diaminocyclohexane).[16] In this compound, the central $[V^{IV}_{15}Sb_6O_{42}(H_2O)]^{6-}$ polyoxoanion is expanded by six in situ generated $[Fe(C_6H_{14}N_2)_2]^{2+}$ complexes, which join neighboring cluster anions into a 3D network via Fe–O bonds.

This representative selection of Sb-POVs showcases the pronounced structure-directed influence of intermolecular interactions in the solid-state lattices and generally the important role of contacts between polyanions and countercations. In this context, we aimed to explore motifs that allow adjustment of the typically high anionic molecular charge of POVs. We here present a novel Sb-POV of composition $[\{Co(teta)_2\}\{Co_2(tren)(teta)_2\}V_{15}Sb_6O_{42}(H_2O)]\cdot ca.9H_2O$ (teta = triethylenetetraamine) featuring direct bonds to cationic moieties: a V–O–Co bond to a binuclear $\{Co_2(tren)(teta)_2\}^{4+}$ unit and a Sb–N covalent bond to the terminal N atom of a bidentate teta ligand in the complex $\{Co(teta)_2\}^{2+}$, a hitherto never observed extension of Sb-POVs.

RESULTS AND DISCUSSION

The compound $\{Co(teta)_2\}[\{Co_2(tren)(teta)_2V_{15}Sb_6O_{42}(H_2O)\}]\cdot ca.9H_2O$ (**1**) crystallizes in the triclinic space group $P\bar{1}$ (see Table S1 in the Supporting Information) with all atoms located on general positions. The central structural motif, $[V_{15}Sb_6O_{42}(H_2O)]^{6-}$, is constructed from 15 distorted VO_5 square pyramids sharing common edges and vertices (Figure 1). Otherwise, the structure can be described as being composed of six VO_5 polyhedra joined by common edges enwrapping three VO_5 units above and below, the same pattern as that observed in other $\{V_{15}Sb_6\}$-containing compounds. The VO_5 polyhedra are bound to six SbO_3 groups via vertices. Two SbO_3 units are joined by a μ_2-O atom to form handle-like Sb_2O_5 moieties. The V–O bonds in the VO_5 square pyramids are characterized by one short bond of the VO^{2+} vanadyl group (ca. 1.6 Å) and four longer bonds at about 1.9–2.0 Å (Table S2 in the Supporting Information). The Sb–O bond lengths are in the range observed for other Sb-POVs [1–16]. Interatomic V···V separations are between 2.85 and 3.07 Å. Bond-valence-sum (BVS) calculations (Table S3 in the Supporting Information) justify the formulation of the cluster anion as $[V^{IV}_{15}Sb^{III}_{6}O_{42}(H_2O)]^{6-}$. The strong absorption of the characteristic V^{IV}=O stretching vibration is located at 961 cm^{-1} in the IR spectrum (Figure S1 in the Supporting Information). Further broad absorptions between about 3600 and 3100 cm^{-1} are caused by the O–H stretching vibration of lattice water molecules and by symmetric and asymmetric N–H modes. The C–H stretching modes of CH_2 are between 2807 and 2992 cm^{-1}, the N–H bending vibration is observed at 1589 cm^{-1}, and the CH_2 bending mode is at 1458 cm^{-1}. The two absorptions at 1070 and 1025 cm^{-1} are most probably caused by C–N stretching modes. Bands below about 750 cm^{-1} cannot be unambiguously assigned because of the overlap of V–O–V and N–H wagging and skeletal vibrations.

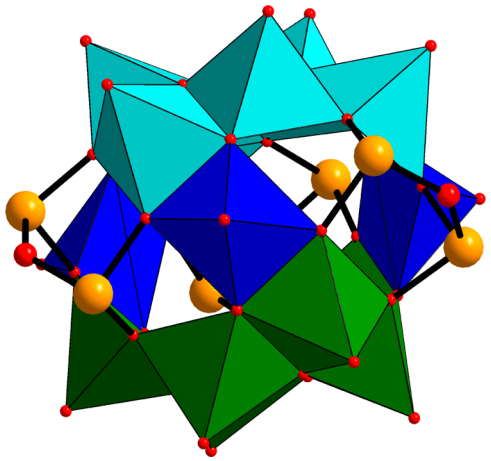

Figure 1. Polyhedral representation of the $[V_{15}Sb_6O_{42}(H_2O)]^{6-}$ cluster. The central V_3 triangle (dark-blue VO_5 pyramids) is sandwiched between two outer V_6 rings of edge-sharing VO_5 pyramids (cyan and green). Color code: Sb, orange spheres; O, red spheres.

In the crystal lattice, two different Co^{2+}-centered complexes are present. The binuclear $\{Co_2(tren)(teta)_2\}^{4+}$ complex consists of two crystallographically unique Co^{2+} cations in different coordination environments. Co1 is surrounded by one tetradentate tren molecule, one N atom of a bridging teta ligand, and one O atom from a VO_5 unit, leading to a distorted CoN_5O octahedron (Table S4 in the Supporting Information). The Co–N bonds between 2.128(8) and 2.162(9) Å (Table S4 in the Supporting Information) are in line with the previously reported data.[11,17−21]

The Co–O bond length of 2.120(5) Å is comparable to those reported for Co–O–V linkages in other POVs.[22−25] The Co1-centered complex is joined to Co2 via a teta ligand acting bidentate to Co2 and monodentate to Co1. To the best of our knowledge, such an interconnection has never been observed before and no example could be found in the Cambridge Structure Database. The environment around Co2 is completed by one tetradentate teta ligand, thus leading to a distorted $Co2N_6$ octahedron (Figure 2, left). The Co2–N bonds can be divided into two groups: four shorter bonds to N atoms in the basal plane of the octahedron [2.154(7)–2.190(8) Å] and two longer bonds to the apical atoms of the polyhedron [2.221(7)–2.228(7) Å] (Table S4 in the Supporting Information), but these values are still comparable with literature data.[11,17−21] The binuclear complex can be formulated as $[Co_2(tren)(teta)_2]^{4+}$, and the connection mode observed here is unique.

In the second complex, the Co3 atom is surrounded by one bidentate and one tetradentate teta ligand to form a distorted

DOI: 10.1021/acs.inorgchem.7b00724
Inorg. Chem. 2017, 56, 7120–7126

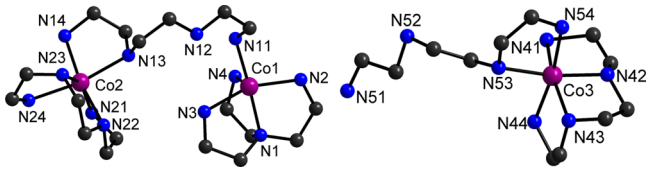

Figure 2. Co^{2+}-centered complexes in the title compound (left and right). Only selected atoms are labeled, and H atoms are omitted for clarity.

octahedron (Table S4 in the Supporting Information and Figure 2, right). The Co−N bonds are between 2.039(17) and 2.248(18) Å and scatter over a larger range than in the dimeric Co^{2+}-centered complex (Table S4 in the Supporting Information).

The cluster anion is expanded by the $V-O_{term}-Co1$ bond to the $\{Co_2(tren)(teta)_2)\}^{4+}$ complex (Figure 3).

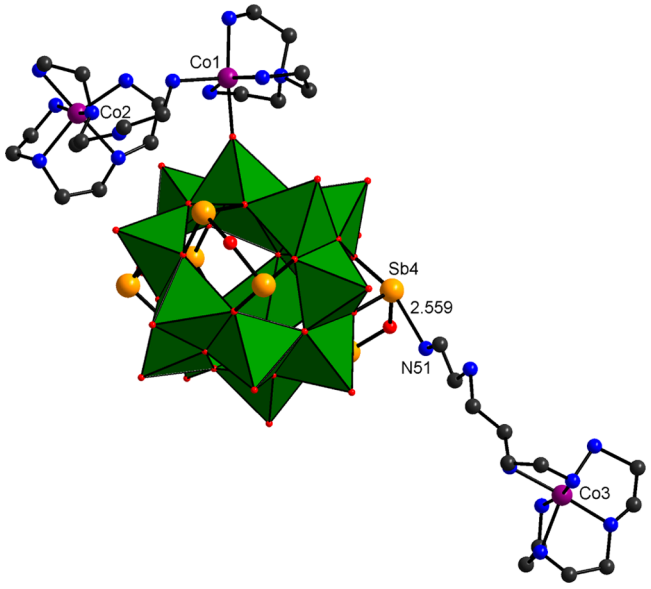

Figure 3. Molecular structure of the title compound. Only selected atoms are labeled, and H atoms are omitted for clarity.

Interestingly, the terminal N atom of the free "arm" of the bidentately acting teta ligand of the Co3 complex has a short contact to an Sb atom (N51−Sb4 = 2.559 Å). Such Sb−N separations were observed in other Sb-POVs, with Sb−N distances ranging from 2.502 to 2.542 Å,[8] raising the question of what type of bond is formed.

A short literature survey demonstrates that Sb−N separation scatterings between about 2 and 2.8 Å are considered as covalent bonds. In the compounds $Sb(phen)Br_3$ and $Sb_2(phen)_4Br_8$, the Sb−N bonds are between 2.239 and 2.408 Å,[26] and in dichloro[*N*(4)-phenyl-2-formylpyridinethiosemicarbazonato]antimony(III), the Sb−N bond lengths are 2.247 and 2.502 Å.[27] Much longer Sb−N bonds ranging from 2.563 to 2.832 Å were reported for $Sb(C_4H_3N_2S)_3{\cdot}^1/_2CH_3OH$.[28] Very short Sb−N bonds of 2.018 and 2.028 Å were observed for $[SbCl(NHMe_2)(\mu\text{-}NBu^t)]$, while a medium-long Sb−N bond is present in $[SbCl_2(NHMe_2)(\mu\text{-}OEt)]_2$ (2.402 Å).[29] Similar medium-long Sb−N distances (2.240 and 2.358 Å) were found for dichloro[*N*(4)-*o*-fluorophenyl2-acetylpyridinethiosemicarbazonato]antimony(III).[30] While the Sb−N distance of 2.029 Å is treated as a covalent bond in $[(\eta^1\text{-}Me_2SiNDipp)NHDippSbCl_2]$ (Dipp = 2,6-diisopropylphenyl), the authors proposed no bonding interaction for the Sb−N separation at 2.66 Å.[31] This short literature survey does not answer the key question of whether the Co3-centered complex is covalently bonded to the cluster anion via a Sb−N bond. However, the electron localization function (ELF), calculated by means of density functional theory (DFT), as shown in Figure 4, demonstrates that the electron distribution along the Sb−N axis has density values similar to those found in the Sb−O bond, i.e., suggesting covalent bonding.

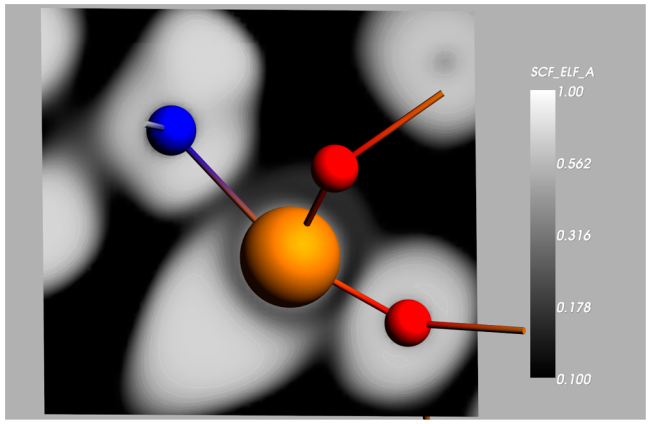

Figure 4. ELF of the Sb−N and Sb−O bonds. The ELF values are given in a gray scale ranging from 0.01 (black) to 1 (white). Color code: orange: Sb; blue, N; red, O.

Natural bond orbital (NBO) analysis also supports the assumption of a covalent Sb−N bond. The orientation and volume occupied by the $5s^2$ orbital are plotted in Figure 5, depicting overlap with the N lone-pair orbital (meshed isosurface).

To have a better understanding about the Sb−N bonding situation in the title compound, we compared the Sb−N bonds in several different compounds [compound **1**, $Sb(C_4H_3N_2S)_3{\cdot}^1/_2CH_3OH$,[28] $[SbCl_2(NHMe_2)(\mu\text{-}OEt)]_2$, and $[SbCl(NHMe_2)(\mu\text{-}NBu^t)]$[29]] because these cover all of the

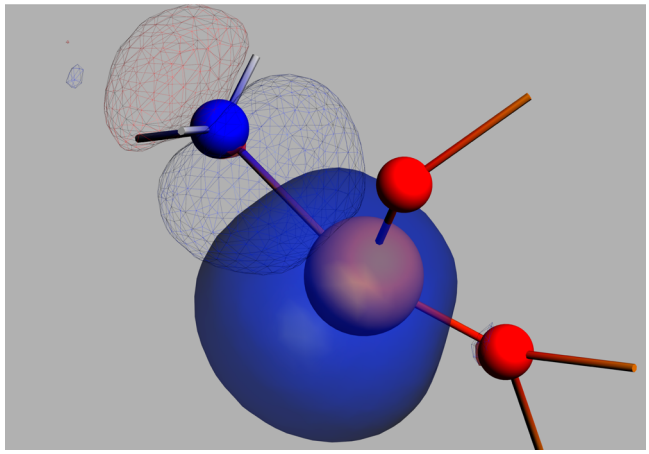

Figure 5. NBO analysis of the title compound. The N lone-pair NLMO (meshed surface) and the $5s^2$ orbital (smooth surface) of the Sb atom are shown. The orbitals are plotted with a threshold value of 0.03 e^-. Only the relevant atoms of the structure are shown.

DOI: 10.1021/acs.inorgchem.7b00724
Inorg. Chem. 2017, 56, 7120−7126

ranges of the Sb−N distances mentioned in the present contribution (see Table 1). The results demonstrate that the

Table 1. Atomic Electron Contributions (Sb and N in %) to All NLMOs Concerned with the Sb−N Bonds (in Å) in the Examples Used as References and in Compound 1[a]

molecule	Sb_x–N_y	NLMO type	bond length	Sb	N
compound **1**	3−190	LP	2.599	4.5	93.3
$Sb(C_4H_3N_2S)_3 \cdot {}^1/_2 CH_3OH$[28]	1−3	LP	2.676	3.4	91.6
	1−8	LP	2.563	4.3	90.6
	1−17	LP	2.833	1.7	93.4
$[SbCl_2(NHMe_2)(\mu\text{-}OEt)]_2$[29]	1−9	LP	2.403	7.8	88.7
	2−10	LP	2.403	7.8	88.7
$[SbCl(NHMe_2)(\mu\text{-}NBu^t)]$[29]	1−4	LP	2.523	6.3	90.3
	1−5	LP	2.018	2.3	92.3
	2−5	LP	2/029	2.0	92.3
	2−29	LP	2.523	6.3	90.3
	1−30	LP	2.029	2.0	92.3
	2−30	LP	2.018	2.3	92.3
	1−5	BD	2.018	20.6	78.3
	1−30	BD	2.018	20.6	78.3
	2−5	BD	2.029	20.7	78.1
	2−30	BD	2.029	20.7	78.1

[a]The structures of the selected compounds used for the calculations are shown in Figure S2 in the Supporting Information. Note that very small contributions from other hybridized orbitals are not listed. The second column lists the atoms involved in a particular bond (x and y being the order number, as listed in Table S5 in the Supporting Information).

bonding between Sb and N atoms is covalent, and it is governed by electron-exchange and donor−acceptor mechanisms. The two mechanisms are reflected in the natural localized molecular orbital (NLMO) types found in the NBO analysis (see Table 1). BD (2-center bond NLMO) corresponds to a bond formed by the electron-exchange mechanism, and LP (lone-pair NLMO) corresponds to the donor−acceptor mechanism. Further examination of the data shows that the Sb−N bonding has NLMOs similar to those of the Sb−N identified as covalent in our reference compounds (see Table 1). The Sb contribution to the lone-pair NLMOs varies between 1.7 and 20.7% depending on the number of Sb−N bonds.

The molecules with the largest extension of about 28 Å are arranged in a layer-like fashion in the (010) plane (Figure 6). Intramolecular C−H···O, N−H···O, and N−H···N interactions (Table S6 in the Supporting Information, geometric parameters in bold) are observed that may stabilize the arrangement of the different constituents. Each molecule is surrounded by six other molecules, and an extended hydrogen-bonding network involving N−H/C−H and O atoms leads to the formation of a 3D arrangement (Table S6 in the Supporting Information). The void space of about 340 $Å^3$ per unit cell is most likely occupied by crystal water molecules.

Upon first heating the material in an inert atmosphere, emission of the crystal water molecules occurs (Δm = 5.1%; Figure S3 in the Supporting Information), indicating the presence of ca. nine water molecules in the sample. After removal of the water molecules, only a very small weight loss is observed up to about 300 °C. Upon further heating, the sample

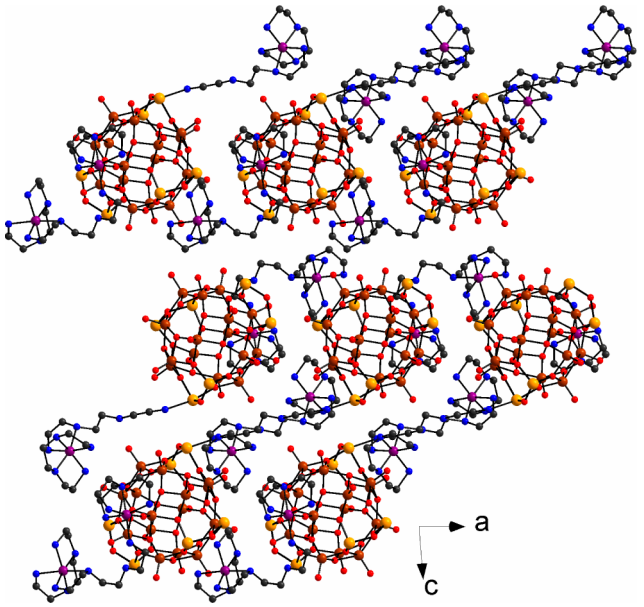

Figure 6. Arrangement of the cluster molecules within the (010) plane.

is decomposed in several not very well-resolved steps up to 850 °C. In a second experiment, heating was stopped at T = 200 °C and an powder X-ray diffraction (XRD) pattern was recorded (Figure S4 in the Supporting Information). The sample is still crystalline, and only shifts of some reflections can be observed, indicating a change of the lattice parameters. In the IR spectrum of the heated sample, the signal of the strong V^{IV}=O stretching vibration at 961 cm^{-1} is still visible, while the absorption between about 3600 and 3400 cm^{-1} is significantly reduced, which is in line with the thermal removal of water molecules (Figure S5 in the Supporting Information). In addition, the absorptions of the ligand molecules are still visible, suggesting that the material is intact after heat treatment at 200 °C.

The UV−vis spectrum of the title compound (Figure S6 in the Supporting Information) exhibits broad absorptions located around 12100 cm^{-1} (1.5 eV), 18400 cm^{-1} (2.28 eV), and 26600 cm^{-1} (3.3 eV). In the energetic region of the first two bands, the $^4T_{1g}(F) \rightarrow {}^4T_{2g}(F)$ and $^4T_{1g}(F) \rightarrow {}^4A_{2g}(F)$ transitions of the Co^{2+} ions and the $^2B_2 \rightarrow {}^2E$, $^2B_2 \rightarrow {}^2B_1$ transitions of the vanadyl group are located, and an unambiguous assignment is not possible. The very intense signal at 3.3 eV is most likely a charge-transfer band.

MAGNETIC PROPERTIES

The magnetic data of compound **1** collected by SQUID measurements are shown in Figure 7 as the temperature dependence of $\chi_m T$ at 0.1 T and as molar magnetization M_m versus magnetic field **B** at 2.0 K. At 290 K, the $\chi_m T$ value of 10.65 cm^3 K mol^{-1} is higher than expected[32] for three noninteracting high-spin Co^{2+} centers (6.94−10.14 cm^3 K mol^{-1}) but significantly below the value that is obtained if the contributions of 15 noninteracting V^{4+} centers are taken into account.

This is, however, expected because of the very strong antiferromagnetic coupling between the spin-$^1/_2$ vanadyl groups in $\{V_{15}Sb_6\}$. Upon lowering of the temperature, the $\chi_m T$ versus T curve is approximately linear down to 170 K, and

DOI: 10.1021/acs.inorgchem.7b00724
Inorg. Chem. 2017, 56, 7120−7126

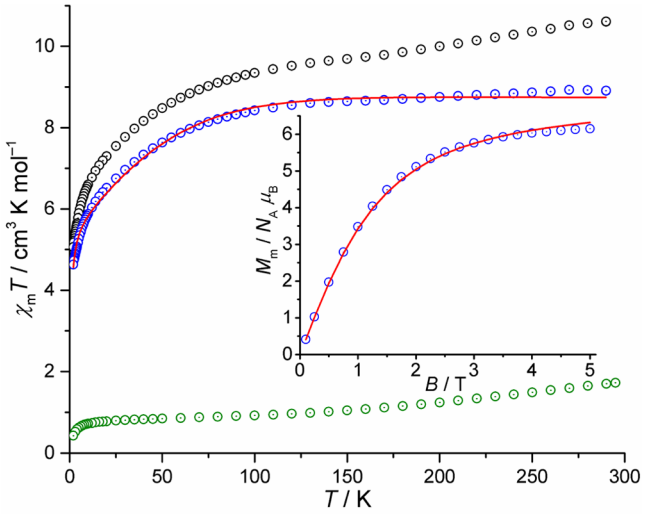

Figure 7. Temperature dependence of $\chi_m T$ for **1**. Inset: Molar magnetization M_m versus applied field **B**. Black circles: experimental data. Green circles: $\chi_m T([V_{15}Sb_6O_{42}]^{6-})$ (scaled). Blue circles: difference of the experimental and $[V_{15}Sb_6O_{42}]^{6-}$ data. Red lines: least-squares fits.

subsequently $\chi_m T$ continuously decreases down to 5.06 cm^3 K mol^{-1} at 2.0 K.

The magnetic properties of the Co^{2+} centers can be approximated by the following assumption: the Co^{2+} sites are considered to be magnetically identical because of their similar coordination environments, and the $Co^{2+}\cdots Co^{2+}$ exchange interactions are expected to be negligible because of their distances and bridging modes, and the interaction between Co1 of $\{Co_2(tren)(teta)_2)\}^{4+}$ and the POV is small because of the very strong antiferromagnetic interactions in $\{V_{15}Sb_6\}$, resulting in a magnetically almost independent spherical spin cluster that is connected to a single Co center. Following these assumptions, the magnetic properties may be determined by subtracting the susceptibility data for an isolated $\{V_{15}Sb_6\}$ cluster [5] until $\chi_m T$ is nearly temperature-independent for $T >$ 200 K. The thus-determined scaling factor of ca. 0.8 reflects differences in the amount of crystal solvents and the cationic lattice. The corresponding scaled contribution for the individual $\{V_{15}Sb_6\}$ polyanion is shown in Figure 7 as green circles, and the remaining contribution from the Co^{2+} centers is shown as blue circles.

To model the magnetic data remaining after the aforementioned subtraction, we use our computational framework *CONDON 2.0*,[33,34] employing a "full model" Hamiltonian. Because of the disorder of the octahedral site symmetries, we assume a site symmetry of C_{4v} introducing the ligand-field parameter B^2_0 besides B^4_0 and B^4_4, with the latter two required for O_h symmetry. To model the Co1–POV exchange interaction, we introduce the mean-field parameter zJ' (z = 1), which has to be small to justify our hypothesis of small exchange interactions and thus our approximation. The simultaneous least-squares fits to $\chi_m T$ versus T and M_m versus B data yield a good goodness-of-fit SQ = 1.3%. The corresponding fits are shown as red lines in Figure 7, and the corresponding model parameters are given in Table S7 in the Supporting Information. We again emphasize that the assumptions made to model the magnetic data can only be understood as a first approximation and the fit parameters should be interpreted accordingly. Notwithstanding the above, the ligand-field parameters represent a ligand field of distorted octahedral symmetry and a ligand-field splitting of 10 Dq ≈ 12000 cm^{-1}. The mean-field parameter zJ' = −0.44 cm^{-1} indicates a small antiferromagnetic exchange interaction between the $\{V_{15}Sb_6\}$ polyanion and the Co1 center. Therefore, the temperature dependence of $\chi_m T$ at T < 150 K is mainly caused by the ligand-field effect of the single Co^{2+} centers, and the exchange interaction affects the $\chi_m T$ versus T curve not until T < 30 K because of its small magnitude.

SUMMARY

Solvothermal synthesis using a mixture of the two isomers tren and teta afforded an expanded Sb-POV with simultaneously formed Sb–N and V–O–Co bonds, a covalent functionalization motif unprecedented in polyoxometalate chemistry. In terms of the bond strength, the Sb–N bonds here are comparable to the Sb–O bonds. The resulting charge neutrality of the complex offers new opportunities for the deposition of such nanosized magnetic molecules on inert substrates without complications associated with countercation aggregation phenomena. As such, this synthesis approach will facilitate future single-molecular charge-transport measurements of such modified Sb-POVs via STM and other methods and thus provide a basis for a systematic study of their molecular spintronics functionality.

EXPERIMENTAL DETAILS

Synthesis. The title compound was prepared in 22 mL glass tubes using 224 mg of NH_4VO_3 (1.9 mmol), 457 mg of Sb_2O_3 (1.57 mmol), and 234 mg of $CoCl_2{\cdot}6H_2O$ (1 mmol) in 2.5 mL of triethylenetetramine (60%) and 1.5 mL of water at 150 °C. The optimal reaction time is 7 days, giving a yield of about 40%. The deep-orange product crystallized as agglomerates of ill-shaped crystals.

Crystal Structure Determination. The intensities were measured using an Imaging Plate Diffraction System (IPDS-2) from STOE using Mo Kα radiation. The crystal structure was solved with the program *SHELXS-2013* and refined against F^2 using *SHELXL-2013*:[35] All non-H atoms, except those of two disordered amine ligands, were refined anisotropically. The C–H and N–H H atoms were positioned with idealized geometry and refined using a riding model. The O–H H atoms of the two water molecules were not located and, thus, not considered in the refinement but in the calculation of the molecular weight. A numerical absorption correction was performed (T_{min}/T_{max} = 0.3351/0.6737). The amine ligands connected to Co3 shows unusually large anisotropic displacement parameters, which can be traced back to disordering, which was refined using a split model. For these atoms, large anisotropic displacement parameters are observed and, therefore, these atoms were refined only isotropically. The disordering remains constant in space group $P1$, and there is no indication for superstructure reflections or any kind of twinning. There is also significant residual electron density directly located at the corresponding Co cation, indicating that the whole complex is disordered. After structure refinement, there is additional residual electron density in the cavities of the structures, which originate from some disordered water molecules. Because no reasonable split model was found, the data were corrected for a disordered solvent using the *SQUEEZE* option in *PLATON*.

CCDC 1499371 contains the supplementary crystallographic data for this paper. These data can be obtained free of charge from the Cambridge Crystallographic Data Centre via http://www.ccdc.cam.ac.uk/data_request/cif.

Energy-Dispersive X-ray (EDX) and Scanning Electron Microscopy (SEM) Analysis. EDX and SEM investigations were performed with a Philips ESEM XL30 environmental scanning electron microscope equipped with an EDAX detector. The ratio of V, Sb, and Co was determined on different single crystals, and the average values are 14.85, 6.15, and 2.95, respectively.

DOI: 10.1021/acs.inorgchem.7b00724
Inorg. Chem. 2017, 56, 7120–7126

Solid-State UV−Vis Spectroscopy. UV−vis spectroscopy investigations were conducted at room temperature using a Cary 5 UV−vis two-channel spectrometer from Varian Techtron Pty., Darmstadt, equipped with an Ulbricht diffuse-reflectance accessory. The optical properties of the compound were investigated by studying the UV−vis reflectance spectrum of the powder sample. $BaSO_4$ was used as a reference material.

IR Spectroscopy. IR spectra (400−4000 cm^{-1}) were recorded with a Bruker Alpha P spectrometer.

Elemental Analysis. CHN analyses were done using a EURO EA elemental analyzer, fabricated by EURO VECTOR Instruments and Software. Experimental data (wt %): C, 11.13; H, 3.36; N, 9.01. Found: C, 11.01; H, 3.45; N, 8.56.

Magnetic Measurement. Magnetic susceptibility data of **1** were measured as a function of the field (0.1−5.0 T) and temperature (2.0−290 K) using a Quantum Design MPMS-5XL SQUID magnetometer. The polycrystalline sample was compacted and immobilized into cylindrical poly(tetrafluoroethylene) capsules. Data were acquired as a function of the field (0.1−5.0 T at 2.0 K) and temperature (2.0−290 K at 0.1 T). The data were corrected for the diamagnetic contributions of the sample holder and the compound ($\chi_{dia} = -1.62 \times 10^{-3}$ cm^3 mol^{-1}).

Theoretical Analysis. We performed DFT calculations and NBO analysis on the title compound. Its geometry was kept as defined by the spectroscopic data. Only the H atomic positions were optimized. For geometry optimization, we employed the PBE[36] functional along with scalar relativistic,[37] long-range (D3)[38] correction, using TZP (for Sb and V), DZP (for C, O, and N), and SZ (for H) Slater-type basis sets.[39] Afterward, the ground-state electronic structure and topological analysis were calculated at the B3LYP[40] level of theory, maintaining the same basis sets and relativistic corrections. Calculations were carried out with the adf2014[41] and NBO6[42] codes. To assess the electron distribution along the Sb−N axis, the ELF[43] was computed.

■ ASSOCIATED CONTENT

Supporting Information

The Supporting Information is available free of charge on the ACS Publications website at DOI: 10.1021/acs.inorgchem.7b00724.

Tables of structural data and refinement results, of interatomic distances, of BVSs for V centers, of atomic coordinates of the model compounds used for theoretical analyses, of intra- and intermolecular hydrogen-bonding interactions, and of parameters used for modeling the magnetic susceptibility data and figures of IR spectra, molecular structures of the model compounds used for theoretical analyses, DTA−TG−DTG curves, XRD patterns of the title compound and after heating to 200 °C, and a UV−vis spectrum (PDF)

Accession Codes

CCDC 1499371 contains the supplementary crystallographic data for this paper. These data can be obtained free of charge via www.ccdc.cam.ac.uk/data_request/cif, or by emailing data_request@ccdc.cam.ac.uk, or by contacting The Cambridge Crystallographic Data Centre, 12 Union Road, Cambridge CB2 1EZ, UK; fax: +44 1223 336033.

■ AUTHOR INFORMATION

Corresponding Author

*E-mail: wbensch@ac.uni-kiel.de. Fax: +49-431-880-1520.

ORCID

Christian Näther: 0000-0001-8741-6508
Paul Kögerler: 0000-0001-7831-3953
Thoma Heine: 0000-0003-2379-6251
Wolfgang Bensch: 0000-0002-3111-580X

Notes

The authors declare no competing financial interest.

■ ACKNOWLEDGMENTS

The authors thank the State of Schleswig-Holstein for financial support. Parts of this work were supported by EU ERC 308051-MOLSPINTRON. The computations were performend at Zentrum für Informationsdienste und Hochleistungsrechnen, Technischen Universität Dresden.

■ REFERENCES

(1) Monakhov, K. Yu.; Bensch, W.; Kögerler, P. Semimetal-functionalised polyoxovanadates. *Chem. Soc. Rev.* **2015**, *44*, 8443−8483.

(2) Zhang, L.; Zhao, X.; Xu, J.; Wang, T. A novel two-dimensional structure containing the first antimony-substituted polyoxovandium clusters: $[\{Co(en)_2\}_2Sb^{III}{}_8V^{IV}{}_{14}O_{42}(H_2O)]\cdot 6H_2O$. *J. Chem. Soc., Dalton Trans.* **2002**, 3275−3276.

(3) Hu, X.-X.; Xu, J.-Q.; Cui, X.-B.; Song, J.-F.; Wang, T.-G. A novel one-dimensional framework material constructed from antimony-substituted polyoxovanadium clusters: $[(C_2N_2H_{10})_2\beta\text{-}\{Sb^{III}{}_8V^{IV}{}_{14}O_{42}(H_2O)\}](C_2N_2H_8)\cdot 4H_2O$. *Inorg. Chem. Commun.* **2004**, *7*, 264−267.

(4) Kiebach, R.; Näther, C.; Bensch, W. $[C_6H_{17}N_3]_4[Sb_4V_{16}O_{42}]\bullet 2H_2O$ and $[NH_4]_4[Sb_8V_{14}O_{42}]\bullet 2H_2O$- the first isolated Sb derivates of the $[V_{18}O_{42}]$ family. *Solid State Sci.* **2006**, *8*, 964−970.

(5) Kiebach, R.; Näther, C.; Kögerler, P.; Bensch, W. $[V^{IV}{}_{15}Sb^{III}{}_6O_{42}]^{6-}$: An antimony analogue of the molecular magnet $[V_{15}As_6O_{42}(H_2O)]^{6-}$. *Dalton Trans.* **2007**, 3221−3223.

(6) Müller, A.; Döring, J. A Novel heterocluster with D_3-symmetry containing 21 core atoms - $[As_6{}^{(III)}V_{15}{}^{(IV)}O_{42}(H_2O)]^{6-}$. *Angew. Chem., Int. Ed. Engl.* **1988**, *27*, 1721.

(7) Wutkowski, A.; Näther, C.; Kögerler, P.; Bensch, W. $[V_{16}Sb_4O_{42}(H_2O)\{VO(C_6H_{14}N_2)_2\}_4]$: A terminal expansion to a polyoxovanadate archetype. *Inorg. Chem.* **2008**, *47*, 1916−1918.

(8) Antonova, E.; Näther, C.; Kögerler, P.; Bensch, W. Organic Functionalization of Polyoxovanadates: Sb-N Bonds and Charge Control. *Angew. Chem., Int. Ed.* **2011**, *50*, 764−767.

(9) Gao, Y.; Han, Z.; Xu, Y.; Hu, C. pH-Dependent Assembly of Two Novel Organic−inorganic Hybrids Based on Vanadoantimonate Clusters. *J. Cluster Sci.* **2010**, *21*, 163−171.

(10) Antonova, E.; Näther, C.; Kögerler, P.; Bensch, W. A C_2-symmetric Antimonato Polyoxovanadate Cluster $[V_{16}Sb_4O_{42}(H_2O)]^{8-}$ derived from the $\{V_{18}O_{42}\}$ archetype. *Dalton Trans.* **2012**, *41*, 6957−6962.

(11) Antonova, E.; Näther, C.; Bensch, W. Assembly of $[V_{15}Sb_6O_{42}(H_2O)]^{6-}$ cluster shells into higher dimensional aggregates via weak Sb···N/Sb···O intercluster interactions and a new polyoxovanadate with a discrete $[V_{16}Sb_4O_{42}(H_2O)]^{8-}$ cluster shell. *CrystEngComm* **2012**, *14*, 6853−6859.

(12) Antonova, E.; Wutkowski, A.; Näther, C.; Bensch, W. Synthesis and structural characterisation of two antimonatopolyoxovanadates containing the $[V_{14}Sb_8O_{42}]$ cluster. *Solid State Sci.* **2011**, *13*, 2154−2159.

(13) Antonova, E.; Näther, C.; Kögerler, P.; Bensch, W. Expansion of Antimonato Polyoxovanadates with Transition Metal Complexes: $(Co(N_3C_5H_{15})_2)_2[\{Co(N_3C_5H_{15})_2\}V_{15}Sb_6O_{42}(H_2O)]\bullet 5\ H_2O$ and $(Ni(N_3C_5H_{15})_2)_2[\{Ni(N_3C_5H_{15})_2\}V_{15}Sb_6O_{42}(H_2O)]\bullet 8\ H_2O$. *Inorg. Chem.* **2012**, *51*, 2311−2317.

(14) Lühmann, H.; Näther, C.; Kögerler, P.; Bensch, W. Solvothermal Synthesis and Crystal Structure of a Heterometal-bridged $\{V_{15}Sb_6\}$ Dimer: $[Ni_2(tren)_3(V_{15}Sb_6O_{42}(H_2O)_{0.5})]_2[Ni(trenH)_2]\cdot H_2O$. *Inorg. Chim. Acta* **2014**, *421*, 549−552.

(15) Antonova, E.; Näther, C.; Bensch, W. Antimonato Polyoxovanadates with Structure Directing Transition Metal Complexes: Pseudopolymorphic $\{Ni(dien)_2\}_3[V_{15}Sb_6O_{42}(H_2O)]\bullet n\ H_2O$ compounds and $\{Ni(dien)_2\}_4[V_{16}Sb_4O_{42}(H_2O)]$. *Dalton Trans.* **2012**, *41*, 1338−1344.

DOI: 10.1021/acs.inorgchem.7b00724
Inorg. Chem. 2017, 56, 7120−7126

(16) Wutkowski, A.; Näther, C.; Kögerler, P.; Bensch, W. An Antimonato-Polyoxovanadate Based Three-Dimensional Framework Exhibiting Ferromagnetic Exchange Interactions: Synthesis, structural characterization and magnetic investigation of $\{[Fe(C_6H_{14}N_2)_2]_3[V_{15}Sb_6O_{42}(H_2O)]\}\bullet 8H_2O$. *Inorg. Chem.* **2013**, *52*, 3280−3284.
(17) Panja, A. Exclusive selectivity of multidentate ligands independent on the oxidation state of cobalt: influence of steric hindrance on dioxygen binding and phenoxazinone synthase activity. *Dalton Trans.* **2014**, *43*, 7760−7770.
(18) Wang, G.-M.; Sun, Y.-Q.; Yang, G.-Y. Syntheses and crystal structures of three new borates templated by transition-metal complexes in situ. *J. Solid State Chem.* **2006**, *179*, 1545−1553.
(19) Liang, J.; Chen, J.; Zhao, J.; Pan, Y.; Zhang, Y.; Jia, D. Solvothermal Syntheses, Crystal Structures, and Thermal Properties of the First Example of Selenidostannates with Mixed Ethylene Polyamine-Coordinated Transition Metal Complexes as Counterions. *Z. Anorg. Allg. Chem.* **2011**, *637*, 445−449.
(20) Zhang, Y.; Zhou, J.; Tang, A.-B.; Bian, G.-Q.; Dai, J. Solvothermal Syntheses and Crystal Structures of Two Thiostannates(IV) $[M(tepa)]_2(\mu\text{-}Sn_2S_6)$ (M = Fe^{2+} and Co^{2+}). *J. Chem. Crystallogr.* **2010**, *40*, 496−500.
(21) Tokarev, K.; Kiskin, M.; Sidorov, A.; Aleksandrov, G.; Bogomyakov, A.; Novotortsev, V.; Eremenko, I. Chemical assembly of an antiferromagnetic macrocyclic molecule containing two inner Co^{II} centers from polymeric cobalt pivalate. *Polyhedron* **2009**, *28*, 2010−2016.
(22) Qi, Y.; Li, Y.; Wang, E.; Zhang, Z.; Chang, S. Metal-controlled self-assembly of arsenic−vanadium-cluster backbones with organic ligands. *Dalton Trans.* **2008**, 2335−2345.
(23) Zhang, C.-D.; Liu, S.-X.; Gao, B.; Sun, C.-Y.; Xie, L.-H.; Yu, M.; Peng, J. Hybrid materials based on metal−organic coordination complexes and cage-like polyoxovanadate clusters: Synthesis, characterization and magnetic properties. *Polyhedron* **2007**, *26*, 1514−1522.
(24) Ollivier, P. J.; De Board, J. R. D.; Zapf, P. J.; Zubieta, J.; Meyer, L. M.; Wang, C.-C.; Mallouk, T. E.; Haushalter, R. C. Hydrothermal synthesis and crystal structures of two novel vanadium oxides containing interlamellar transition metal complexes. *J. Mol. Struct.* **1998**, *470*, 49−60.
(25) Zhou, G.; Xu, Y.; Guo, C.; Zheng, X. Hydrothermal synthesis, characterization and magnetic properties of a new 2D arsenic−vanadate layers supported cobalt coordination complex: $[Co(en)_2(H_2O)]\{[Co(en)_2]_2As_8V_{14}O_{42}(SO_4)\} \cdot 3H_2O$. *Inorg. Chem. Commun.* **2007**, *10*, 849−852.
(26) Yin, H. D.; Zhai, J. Synthesis, characterizations and crystal structures of antimony(III) complexes with nitrogen-containing ligands. *Inorg. Chim. Acta* **2009**, *362*, 339−345.
(27) Lessa, J. A.; Reis, D. C.; Mendes, I. C.; Speziali, N. L.; Rocha, L. F.; Pereira, V. R. A.; Melo, C. M. L.; Beraldo, H. Antimony(III) complexes with pyridine-derived thiosemicarbazones: Structural studies and investigation on the antitrypanosomal activity. *Polyhedron* **2011**, *30*, 372−380.
(28) Hadjikakou, S. K.; Antoniadis, C. D.; Hadjiliadis, N.; Kubicki, M.; Binolis, J.; Karkabounas, S.; Charalabopoulos, K. Synthesis and characterization of new water stable antimony(III) complex with pyrimidine-2-thione and in vitro biological study. *Inorg. Chim. Acta* **2005**, *358*, 2861−2866.
(29) Edwards, A. J.; Leadbeater, N. E.; Paver, M. A.; Raithby, P. R.; Russell, C. A.; Wright, D. S. Dimeric antimony complexes capturing dimethylamine as a neutral donor; syntheses and structural characterisation of $[SbCl_2(NHMe_2)(\mu\text{-}OEt)]_2$ and $[SbCl(NHMe_2)(\mu\text{-}NBu^t)]_2$. *J. Chem. Soc., Dalton Trans.* **1994**, 1479−1482.
(30) Parrilha, G. L.; Dias, R. P.; Rocha, W. R.; Mendes, I. C.; Benítez, D.; Varela, J.; Cerecetto, H.; González, M.; Melo, C. M. L.; Neves, J. K. A. L.; Pereira, V. R. A.; Beraldo, H. 2-Acetylpyridine- and 2-benzoylpyridine-derived thiosemicarbazones and their antimony(III) complexes exhibit high anti-trypanosomal activity. *Polyhedron* **2012**, *31*, 614−621.
(31) Ma, X.; Ding, Y.; Roesky, H. W.; Sun, S.; Yang, Z. Synthesis and Crystal Structures of Antimony(III) Complexes With a Bis(amino)-silane Ligand. *Z. Anorg. Allg. Chem.* **2013**, *639*, 49−52.
(32) Lueken, H. *Magnetochemie*; Teubner Verlag: Stuttgart, Germany, 1999.
(33) Speldrich, M.; Schilder, H.; Lueken, H.; Kögerler, P. A Computational Framework for Magnetic Polyoxometalates and Molecular Spin Structures: CONDON 2.0. *Isr. J. Chem.* **2011**, *51*, 215−227.
(34) van Leusen, J.; Speldrich, M.; Schilder, H.; Kögerler, P. Comprehensive Insight into Molecular Magnetism via CONDON: Full vs. Effective Models. *Coord. Chem. Rev.* **2015**, *289−290*, 137−148.
(35) Sheldrick, G. M. A short history of *SHELX*. *Acta Crystallogr., Sect. A: Found. Crystallogr.* **2008**, *64*, 112−122.
(36) Perdew, J. P.; Burke, K.; Ernzerhof, M. Generalized Gradient Approximation Made Simple. *Phys. Rev. Lett.* **1996**, *77*, 3865−3868.
(37) (a) Becke, A. D. A new mixing of Hartree−Fock and local density-functional theories. *J. Chem. Phys.* **1993**, *98*, 1372−1377. (b) Stephens, P. J.; Devlin, F. J.; Chabalowski, C. F.; Frisch, M. J. Ab Initio Calculation of Vibrational Absorption and Circular Dichroism Spectra Using Density Functional Force Fields. *J. Phys. Chem.* **1994**, *98*, 11623−11627.
(38) Van Lenthe, E.; Baerends, E. J.; Snijders, J. G. Relativistic regular two-component Hamiltonians. *J. Chem. Phys.* **1993**, *99*, 4597−4610.
(39) Grimme, S.; Antony, J.; Ehrlich, S.; Krieg, H. A consistent and accurate ab initio parametrization of density functional dispersion correction (DFT-D) for the 94 elements H-Pu. *J. Chem. Phys.* **2010**, *132*, 154104.
(40) Van Lenthe, E.; Baerends, E. J. Optimized Slater-type basis sets for the elements 1−118. *J. Comput. Chem.* **2003**, *24*, 1142−1156.
(41) Autschbach, J.; Bashford, D.; Brces, A.; Bickelhaupt, F. M.; Bo, C.; Boerrigter, P. M.; Cavallo, L.; Chong, D. P.; Deng, L.; Dickson, R. M.; Ellis, D. E.; van Faassen, M.; Fan, L.; Fischer, T. H.; Fonseca Guerra, C.; Ghysels, A.; Giammona, A.; van Gisbergen, S. J. A.; Götz, A. W.; Groeneveld, J. A.; Gritsenko, O. V.; Grüning, M.; Gusarov, S.; Harris, F. E.; van den Hoek, P.; Jacob, C. R.; Jacobsen, H.; Jensen, L.; Kaminski, J. W.; van Kessel, G.; Kootstra, F.; Kovalenko, A.; Krykunov, M. V.; Van Lenthe, E.; McCormack, D. A.; Michalak, A.; Mitoraj, M.; Neugebauer, J.; Nicu, V. P.; Noodleman, L.; Osinga, V. P.; Patchkovskii, S.; Philipsen, P. H. T.; Post, D.; Pye, C. C.; Ravenek, W.; Rodriguez, J. I.; Ros, P.; Schipper, P. R. T.; Schreckenbach, G.; Seldenthuis, J. S.; Seth, M.; Snijders, J. G.; Sol, M.; Swart, M.; Swerhone, D.; te Velde, G.; Vernooijs, P.; Versluis, L.; Visscher, L.; Visser, O.; Wang, F.; Wesolowski, T. A.; van Wezenbeek, E. M.; Wiesenekker, G.; Wolff, S. K.; Woo, T. K.; Yakovlev, A. L.; Baerends, E. J.; Ziegler, T. *ADF2012, SCM, Theoretical Chemistry*; Vrije Universiteit, Amsterdam, The Netherlands, 2012; http://www.scm.com.
(42) Glendening, E. D.; Badenhoop, J. K.; Reed, A. E.; Carpenter, J. E.; Bohmann, J. A.; Morales, C. M.; Weinhold, F. *NBO*, version 6.0; Theoretical Chemistry Institute, University of Wisconsin: Madison, WI, 2013; http://nbo6.chem.wisc.edu/.
(43) Becke, A. D.; Edgecombe, K. E. A simple measure of electron localization in atomic and molecular systems. *J. Chem. Phys.* **1990**, *92*, 5397−5403.

DOI: 10.1021/acs.inorgchem.7b00724
Inorg. Chem. 2017, 56, 7120−7126